UNIVERSITY OF BIRMINGHAM
University of Birmingham Research at Birmingham

Single-molecule imaging reveals receptor-G protein interactions at cell surface hot spots

Sungkaworn, Titiwat; Jobin, Marie-Lise; Burnecki, Krzysztof; Weron, Aleksander; Lohse, Martin J.; Calebiro, Davide

DOI:
10.1038/nature24264

License:
None: All rights reserved

Document Version
Peer reviewed version

Citation for published version (Harvard):
Sungkaworn, T, Jobin, M-L, Burnecki, K, Weron, A, Lohse, MJ & Calebiro, D 2017, 'Single-molecule imaging reveals receptor-G protein interactions at cell surface hot spots', *Nature*, vol. 550, pp. 543-547. https://doi.org/10.1038/nature24264

Link to publication on Research at Birmingham portal

Publisher Rights Statement:
Published in Nature, volume 550, pages 543–547 (26 October 2017)
doi:10.1038/nature24264

General rights
Unless a licence is specified above, all rights (including copyright and moral rights) in this document are retained by the authors and/or the copyright holders. The express permission of the copyright holder must be obtained for any use of this material other than for purposes permitted by law.

•Users may freely distribute the URL that is used to identify this publication.
•Users may download and/or print one copy of the publication from the University of Birmingham research portal for the purpose of private study or non-commercial research.
•User may use extracts from the document in line with the concept of 'fair dealing' under the Copyright, Designs and Patents Act 1988 (?)
•Users may not further distribute the material nor use it for the purposes of commercial gain.

Where a licence is displayed above, please note the terms and conditions of the licence govern your use of this document.

When citing, please reference the published version.

Take down policy
While the University of Birmingham exercises care and attention in making items available there are rare occasions when an item has been uploaded in error or has been deemed to be commercially or otherwise sensitive.

If you believe that this is the case for this document, please contact UBIRA@lists.bham.ac.uk providing details and we will remove access to the work immediately and investigate.

Download date: 24. Apr. 2024

Single-molecule imaging reveals receptor-G protein interactions at cell surface hot spots

Titiwat Sungkaworn[1,2], Marie-Lise Jobin[1,2], Krzysztof Burnecki[3], Aleksander Weron[3], Martin J. Lohse[1,2,†], Davide Calebiro[1,2,4,5*]

[1]Institute of Pharmacology and Toxicology and [2]Bio-Imaging Center/Rudolf Virchow Center, University of Würzburg, Germany

[3]Faculty of Pure and Applied Mathematics, Hugo Steinhaus Center, Wroclaw University of Science and Technology, Poland

[4]Institute of Metabolism and Systems Research, University of Birmingham, Birmingham, UK

[5]Centre of Membrane Proteins and Receptors (COMPARE), Universities of Birmingham and Nottingham, UK

[†]Present address: Max Delbrück Center for Molecular Medicine, Berlin, Germany

* address correspondence to:

Davide Calebiro, Institute of Pharmacology and Toxicology, Versbacher Str. 9,

97078 Würzburg, Germany – E-mail: davide.calebiro@toxi.uni-wuerzburg.de

G protein-coupled receptors (GPCRs) mediate the biological effects of many hormones and neurotransmitters and are major pharmacological targets[1]. They transmit their signals to the cell interior via interaction with G proteins. However, how receptors and G proteins meet, interact and couple is still ill understood. Here, we analyse the concerted motion of GPCRs and G proteins on the plasma membrane and provide a quantitative model that reveals the key factors at the basis of the high spatiotemporal complexity of their interactions. Using two-colour, single-molecule imaging we visualize interactions between individual receptors and G proteins at the surface of living cells. Under basal conditions, receptors and G proteins form activity-dependent complexes that last for ~1 second. Different agonists specifically regulate the kinetics of receptor-G protein interactions, mostly increasing their association rate. We find hot spots on the plasma membrane, at least partially defined by the cytoskeleton and clathrin-coated pits, where receptors and G proteins are confined and preferentially couple. Imaging with the nanobody Nb37 suggests that signalling preferentially occurs at these hot spots. These findings shed new light on the dynamic interactions governing GPCR signalling.

Different scenarios have been developed to explain how receptors and G proteins interact[2,3]. However, key questions concerning the stability of these interactions and the occurrence of GPCR signalling subdomains at the plasma membrane are still open (see also Supplementary Discussion). To address these questions, we visualized individual receptors and G proteins at the surface of living cells with high spatial (≈20 nm) and temporal (≈30 ms) resolution[4]. As a model, we chose the α_{2A}-adrenergic receptor (α_{2A}-AR), a prototypical family-A GPCR with strong G_i coupling[2]. The α_{2A}-AR and a pertussis toxin (PTX)-insensitive $G\alpha_{i1}$ construct were specifically labelled with two different organic fluorophores via a SNAP[5] or CLIP[6] tag, respectively (Fig. 1a); both constructs were fully functional (Extended Data Fig. 1a, b). These constructs were transiently expressed at low physiological densities (0.55±0.10 and 0.51±0.09 molecule μm^{-2}, respectively) in CHO cells – cultured with PTX to inactivate endogenous $G_{i/o}$ proteins – and simultaneously imaged by fast two-colour single-molecule microscopy combined with single-particle tracking[4] (Fig. 1b and Supplementary Videos 1 and 2). Labelling efficiencies were ~90% (extracellular) and ~80% (intracellular); non-specific labelling was <1% (Extended Data Fig. 1c-e).

Individual α_{2A}-AR trajectories were evaluated by mean square displacement (MSD) analysis (corrected for localization error, see Supplementary Methods), which revealed a high heterogeneity and features of anomalous diffusion[7]. Under basal conditions, 11% of the receptors were virtually immobile, while 38% had sub-, 45% normal and 6% super-diffusion (i.e. directional motion) (Extended Data Fig. 2). $G\alpha_i$ had a significantly different diffusion pattern, with a larger immobile fraction (37%) (Extended Data Fig. 2c, d). Stimulation with the full agonist norepinephrine (NE) or brimonidine (UK-14,304) caused a small, significant change in the overall diffusion pattern of $G\alpha_i$ but not of α_{2A}-AR (Extended Data Fig. 2d). Similar results were obtained for a second receptor/G protein pair, i.e. β_2-adrenergic receptor (β_2-AR) and $G\alpha_s$, but no significant differences were observed upon stimulation with the full agonist isoproterenol (Iso; Extended Data Fig. 2d).

We then analysed the trajectories with an algorithm based on hidden Markov models (HMMs)[8], which assumes that particles switch among discrete diffusive states following a stochastic process. We found that both receptors and G proteins frequently switched among at least four distinguishable states (S1 to S4), characterized by distinct diffusion coefficients (*D*) and ranging from a virtually immobile (S1) to a fast diffusive (S4) state (Fig. 1c-f and Extended Data Fig. 3). The results were overall consistent with those of the MSD analysis. We hypothesized that the two slowest states (S1 and S2) were due to trapping in small membrane compartments and, based on the corresponding *D* and average dwell times, we estimated compartment radiuses of <50 nm and ~270 nm, respectively (see Supplementary Methods). Although with some differences, a similar picture was observed for the integral membrane protein CD86 – used as control[4] (Fig. 1f, Extended Data Figs. 2d and 3), indicating that such diffusion behaviour is not unique to GPCRs/G proteins.

Density maps of single-molecule localizations revealed areas that were either preferentially explored or avoided by α_{2A}-ARs and $G\alpha_i$ subunits (Extended Data Fig. 4a and Supplementary Video 3). To better characterize these areas, we generate dynamic maps from the trajectories, reporting local *D* and potential energy (*V*) values[9]. This analysis revealed a complex dynamic landscape at the plasma membrane, with high-potential areas, which were rapidly left by α_{2A}-ARs/$G\alpha_i$ subunits, and low-potential areas, where they tended to be trapped (Extended Data Fig. 4b, dark areas; see Extended Data Fig. 1f for control). There was a partial but consistent overlap between the potential energy maps of α_{2A}-ARs and $G\alpha_i$ subunits (Extended Data Fig. 4c). To quantify this, we measured the relative potential energy values ($V_{L,rel}$) of $G\alpha_i$ at the sites of α_{2A}-AR localization and vice versa, which were both significantly lower than for random

localizations or compared to CD86 (Fig. 2a). Importantly, receptor:G protein interactions preferentially occurred at the shared low potential energy areas ("hot spots"), as indicated by negative $V_{L,rel}$ values (Fig. 2b). Similar results were obtained for β_2-AR and $G\alpha_s$ (Extended Data Fig. 5a, b).

To investigate possible factors responsible for this complex diffusion dynamics, we imaged both the cytoskeleton and clathrin-coated pits (CCPs) underneath the plasma membrane. α_{2A}-ARs trajectories tended to avoid microtubules and actin fibres, as suggested by negative colocalization index values (Fig 2c, d, Supplementary Videos 4 and 5), in agreement with the fence-and-picket model[10]. Moreover, the majority of trajectories tended to avoid CCPs (Fig. 2e, Supplementary Video 6). This coexisted with a minor fraction of α_{2A}-ARs that either transiently stopped at CCPs (Fig. 2f, arrowheads) – consistent with receptor recruitment to pre-existing CCPs[11] – or were immobile and localized at CCPs. The fraction of CCPs occupied by α_{2A}-ARs increased upon agonist stimulation (Fig. 2f, right), Overlays of single particle trajectories with superresolved actin images, obtained by photoactivated localization microscopy (PALM)[12], suggested that the actin mesh underneath the plasma membrane created sub-micrometre compartments in which α_{2A}-ARs were apparently loosely trapped (Fig. 2g and Supplementary Video 7; radius ~100-300 nm, in agreement with estimation based on HMM analysis). Consistently, superimposition of PALM images with potential energy maps showed that the low potential areas were often at least partially delimited by actin fibres (Fig. 2h and Extended Data Fig. 4d). Similar results were obtained for β_2-AR (Extended Data Fig. 5c-f) and $G\alpha_i$ (Extended Data Fig. 6 and Supplementary Video 8).

Next, we developed a mathematical analysis to estimate the duration of receptor:G protein interactions based on their trajectories. We reasoned that, on average, for two particles undergoing a true interaction, their observed colocalization time (Δt_{obs}) should correspond to the average duration of true interactions (Δt_{true}) plus the average duration of random colocalizations (Δt_{random}) (Fig. 3a and Extended Data Fig. 7). Thus, we deconvolved the observed colocalization times with those of random colocalizations (obtained with CD86 and $G\alpha_i$) to estimate the distribution of the underlying true receptor:G protein interactions (Fig. 3b and Supplementary Methods). The results were subsequently expressed as normalized relaxation curves, showing the fraction of the interactions that are still ongoing at time t from the beginning of each interaction (Fig. 3c). The very fast component in Fig. 3b, seen also with the control CD86, corresponds to non-productive interactions plus random colocalizations, the rate of which (k_{np+rc}) did not differ among the conditions tested (Fig. 3d, left), while we considered the remainder to

be productive interactions, i.e. interactions that result in the formation of a “true” complex (see Supplementary Discussion). α_{2A}-ARs and Gα_i underwent some productive interactions already under basal conditions (Fig. 3b, c). A major fraction of these interactions terminated following an exponential decay, while a very small fraction (approximately $3 \cdot 10^{-4}$) was stable over the observation time (Fig. 3c). From a fitting of the major component in Fig. 3c and the particle densities we estimated an association rate constant (k_{on}) of ~0.015 μm^2 molecule^{-1} s^{-1} and a dissociation rate constant (k_{off}) of ~0.8 s^{-1} for the productive interactions under basal conditions (Fig. 3d, middle/right). Treatment with an inverse agonist (yohimbine) or Gα_i inactivation (using a PTX-sensitive construct) suppressed the major fraction of transient productive interactions, suggesting that they resulted from constitutive α_{2A}-AR activity and required a functional Gα_i subunit; in contrast, the small fraction of stable productive interactions was not affected (Fig. 3e). Stimulation with norepinephrine caused a concentration-dependent increase of k_{on} up to ~0.2 μm^2 molecule^{-1} s^{-1}, while k_{off} was only marginally affected (Fig. 3b-d). This translates into 2-dimensional equilibrium dissociation constants (K_d) of ~50 and 6 molecule μm^{-2} for basal and stimulated conditions, respectively. Based on these results, we estimated that, at the tested densities, ~0.5% (basal) or 5% (stimulated) of all α_{2A}-ARs were in complex with Gα_i at any given time. Similar results were obtained for β_2-AR:Gα_s interactions, although with 10-fold lower k_{on} values and no long-lived interactions (Fig. 3f, g). A panel of α_{2A}-AR agonists with varying efficacy and affinity revealed statistically significant differences in the estimated k_{on} and, to a lesser extent, k_{off} values (Fig. 3d). Overall, there was a positive correlation between k_{on} and efficacy (Fig. 3h). However, there was also a trend towards smaller k_{on} values for higher affinity agonists, both considering full (UK-14,304 vs. norepinephrine) or partial (clonidine vs. oxymetazoline) agonists with comparable efficacies and dissimilar affinities (Fig. 3d, h).

By visually inspecting the trajectories, we observed that several α_{2A}-ARs and Gα_i subunits slowed down or stopped during apparent interactions to then either remain confined or resume their motion (Fig. 3i, Fig 3j, left and Supplementary Video 9), while the remainder retained their mobility (Fig. 3j, right). A quantitative analysis of the HMM states of α_{2A}-AR and Gα_i trajectories showed that, during the time of interaction, higher fractions of receptors/G proteins were in states S1 (virtually immobile) and S2 (slowly diffusing) (Fig. 3k). These mobility changes occurring during the short interaction times and the global changes in Gα_i diffusion described in Extended Data Fig. 2d and 3 likely represent distinct phenomena.

To further validate our results, we performed deterministic simulations of GPCR signalling using the estimated microscopic k_{on} and k_{off} values for receptor:G protein interactions. The results

were in very good agreement with ensemble (FRET) measurements of α_{2A}-AR/G_i association/dissociation (Extended Data Fig. 8). These simulations also suggested that G protein signalling can be fast only if it occurs while the G protein is still bound to the receptor (Supplementary Data). Moreover, we performed particle-based stochastic simulations of receptors and G proteins diffusing and interacting on a 2D surface (Fig 4a). Introducing the experimentally measured potential energy (*V*) landscapes (as in Fig. 2b) in these simulations doubled the probability of receptor:G protein interactions compared to conditions of simple Brownian motion (Fig. 4a).

To investigate whether hot spots for receptor:G protein interactions also occur in a more physiological context, we studied primary human endothelial cells (HUVEC), where both α_{2A}- and β_2-ARs are endogenously expressed and regulate vascular tone[13]. We found that in these cells both α_{2A}-AR:Gα_i and β_2-AR:Gα_s interactions were preferentially occurring at low potential energy areas (Extended Data Fig. 9a, b). We also found that receptors and G proteins slowed down or stopped moving during their interactions (Extended Data Fig. 9c), further strengthening our observations in CHO cells.

Finally, we assessed G_s activation using the conformation-sensitive nanobody Nb37[14,15], which recognizes the active (nucleotide-free) state of Gα_s. In HUVEC transfected with Nb37 fused to a fluorescent protein (EYFP), Nb37 preferentially localized at the sites where β_2-ARs were concentrated (Fig. 4b).

The main findings of our study are summarized in Extended Data Figure 10. First, our results reveal a complex picture, whereby barriers, at least partially constituted by actin fibres, microtubules and CCPs, contribute to the formation of hot spots where receptors and G proteins are both concentrated, and where G protein coupling as well as signalling preferentially occur. This provides a direct visualization of previously postulated GPCR signalling nanodomains[16,17]. Based on our results and simulations, we hypothesize that this complex organization increases both the speed and efficiency of receptor:G protein coupling, while allowing G protein signalling to occur locally.

Second, our data provide direct estimates of the frequency and duration of receptor:G protein interactions in living cells. We find that most receptor:G protein interactions are short-lived (lifetime ~1-2 s). The dependency of these complexes on receptor activation suggests that they are linked to signalling, which is further supported by the observation that G protein activation occurs preferentially at the sites of interaction. In addition, we observe a very small fraction of

long-lived complexes (lifetime >> 4s), possibly corresponding to those reported in previous studies[3,18]. The coexistence of short- and long-lived complexes might reconcile earlier contrasting data. Intriguingly, the estimated duration of the short-lived interactions is much longer than the time required for effector activation, which can happen in ~40 ms[2]. Thus, as suggested by our deterministic simulations, it is conceivable that fast effector activation might occur while the G protein is still bound to the receptor[19].

Third, our results reveal that receptor:G protein interactions are regulated by agonists largely at the level of k_{on}. The low k_{on} values measured here also indicate that random collisions only seldom lead to the formation of productive receptor:G protein complexes. The fact that k_{on} is regulated by agonists and the low k_{on} values suggest that receptor:G protein interactions are not limited by diffusion, but rather by the major conformational changes occurring during the formation of receptor:G protein complexes[14,20-22] (see also Supplementary Discussion). Interestingly, different agonists induce substantially different k_{on} values, which correlate at least partially with their efficacies. Together with small differences in the k_{off} values, these findings suggest the possibility of fine-tuning receptor signalling using drugs with tailored effects on the kinetics of receptor:G protein interactions. Finally, our finding of lower k_{on} values for β_2-AR:Gα_s than for α_{2A}-AR:Gα_i interactions is consistent with the view that coupling to G_s might require a larger conformational change than coupling to G_i[23].

In summary, our single-molecule results reveal new key factors involved in the regulation of receptor:G protein interactions, which may allow modifying receptor signalling in ways that far exceed simple receptor blockade or activation achieved with currently available drugs, for example by modulating the on/off rates of receptor:G protein interactions or manipulating receptor/G protein mobility and coupling at the hot spots. They further illustrate how GPCR signalling results from dynamic interactions among receptors, G proteins and the complex surrounding membrane environment, which confers flexibility and versatility to this fundamental biological process.

References

1 Pierce, K. L., Premont, R. T. & Lefkowitz, R. J. Seven-transmembrane receptors. *Nat. Rev. Mol. Cell. Biol.* **3**, 639-650 (2002).

2 Hein, P., Frank, M., Hoffmann, C., Lohse, M. J. & Bünemann, M. Dynamics of receptor/G protein coupling in living cells. *EMBO J.* **24**, 4106-4114 (2005).

3 Galès, C. *et al.* Probing the activation-promoted structural rearrangements in preassembled receptor-G protein complexes. *Nat. Struct. Mol. Biol.* **13**, 778-786 (2006).

4 Calebiro, D. *et al.* Single-molecule analysis of fluorescently labeled G-protein-coupled receptors reveals complexes with distinct dynamics and organization. *Proc. Natl. Acad. Sci. U. S. A.* **110**, 743-748 (2013).

5 Keppler, A. *et al.* A general method for the covalent labeling of fusion proteins with small molecules in vivo. *Nat. Biotechnol.* **21**, 86-89 (2003).

6 Gautier, A. *et al.* An engineered protein tag for multiprotein labeling in living cells. *Chem. Biol.* **15**, 128-136 (2008).

7 Magdziarz, M., Weron, A., Burnecki, K. & Klafter, J. Fractional Brownian motion versus the continuous-time random walk: a simple test for subdiffusive dynamics. *Phys. Rev. Lett.* **103**, 180602 (2009).

8 Persson, F., Linden, M., Unoson, C. & Elf, J. Extracting intracellular diffusive states and transition rates from single-molecule tracking data. *Nat. Methods* **10**, 265-269 (2013).

9 El Beheiry, M., Dahan, M. & Masson, J.-B. InferenceMAP: mapping of single-molecule dynamics with Bayesian inference. *Nat. Methods* **12**, 594-595 (2015).

10 Kusumi, A., Shirai, Y. M., Koyama-Honda, I., Suzuki, K. G. & Fujiwara, T. K. Hierarchical organization of the plasma membrane: investigations by single-molecule tracking vs. fluorescence correlation spectroscopy. *FEBS Lett.* **584**, 1814-1823 (2010).

11 Scott, M. G., Benmerah, A., Muntaner, O. & Marullo, S. Recruitment of activated G protein-coupled receptors to pre-existing clathrin-coated pits in living cells. *J. Biol. Chem.* **277**, 3552-3559 (2002).

12 Betzig, E. *et al.* Imaging intracellular fluorescent proteins at nanometer resolution. *Science* **313**, 1642-1645 (2006).

13 Vanhoutte, P. M. Endothelial adrenoceptors. *J. Cardiovasc. Pharmacol.* **38**, 796-808 (2001).

14 Rasmussen, S. G. *et al.* Crystal structure of the β_2 adrenergic receptor-G_s protein complex. *Nature* **477**, 549-555 (2011).

15 Irannejad, R. *et al.* Conformational biosensors reveal GPCR signalling from endosomes. *Nature* **495**, 534-538 (2013).

16 Insel, P. A. *et al.* Compartmentation of G-protein-coupled receptors and their signalling

components in lipid rafts and caveolae. *Biochem. Soc. Trans.* **33**, 1131-1134 (2005).

17 Pontier, S. M. *et al.* Cholesterol-dependent separation of the β_2-adrenergic receptor from its partners determines signaling efficacy: insight into nanoscale organization of signal transduction. *J. Biol. Chem.* **283**, 24659-24672 (2008).

18 Qin, K., Dong, C., Wu, G. & Lambert, N. A. Inactive-state preassembly of G_q-coupled receptors and G_q heterotrimers. *Nat. Chem. Biol.* **7**, 740-747 (2011).

19 Rebois, R. V. *et al.* Heterotrimeric G proteins form stable complexes with adenylyl cyclase and Kir3.1 channels in living cells. *J. Cell. Sci.* **119**, 2807-2818 (2006).

20 Westfield, G. H. *et al.* Structural flexibility of the $G\alpha_s$ α-helical domain in the β_2-adrenoceptor G_s complex. *Proc. Natl. Acad. Sci. U. S. A.* **108**, 16086-16091 (2011).

21 Dror, R. O. *et al.* Structural basis for nucleotide exchange in heterotrimeric G proteins. *Science* **348**, 1361-1365 (2015).

22 Gregorio, G. G. *et al.* Single-molecule analysis of ligand efficacy in β_2AR–G-protein activation. *Nature* **547**, 68-73 (2017).

23 Rose, A. S. *et al.* Position of transmembrane helix 6 determines receptor G protein coupling specificity. *J. Am. Chem. Soc.* **136**, 11244-11247 (2014).

24 Nikolaev, V. O., Hoffmann, C., Bunemann, M., Lohse, M. J. & Vilardaga, J. P. Molecular basis of partial agonism at the neurotransmitter α_{2A}-adrenergic receptor and G_i-protein heterotrimer. *J. Biol. Chem.* **281**, 24506-24511 (2006).

Supplementary Information is linked to the online version of the paper at www.nature.com/nature.

Acknowledgements We thank Steve P. Watson, Markus Sauer, Carlo Manzo and Emanuele Cocucci for helpful discussions. This work was supported by a grant of the Deutsche Forschungsgemeinschaft (Sonderforschungsbereich/Transregio 166–Project C1 to D.C.) and in part by funds of the Deutsche Forschungsgemeinschaft (grant CA 1014/1-1 to D.C. and FZT82 Rudolf Virchow Center to M.J.L.), the IZKF Würzburg (grant B-281 to D.C.), the European Research Council (Advanced Grant 232944–TOPAS to M.J.L.) and the Polish National Science Center (Maestro Grant No. 2012/06/A/ST1/00258 to K.B. and A.W.). T.S. was in part supported

by an Alexander-von-Humboldt/Bayer Foundation fellowship.

Author contributions T.S. and M-L.J. performed the experiments. T.S., M-L.J., K.B. and D.C. analysed the data. K.B., A.W. and D.C. developed the mathematical analyses. D.C. wrote the software. D.C. and T.S. wrote the manuscript with contribution of M.J.L. All authors discussed the results. D.C. conceived and supervised the study.

Author information Reprints and permissions information is available at www.nature.com/reprints. The authors declare no competing financial interests. Correspondence and requests for materials should be addressed to D.C. (davide.calebiro@toxi.uni-wuerzburg.de).

Figure Legends

Figure 1 | Single-molecule imaging of receptors/G proteins. a, Overall strategy. The α_{2A}-AR was labelled with S549-BG via a SNAP tag fused to its N-terminus. The G_i protein was labelled with SiR-BC via a CLIP tag inserted in an internal loop of the $G\alpha_i$ subunit. **b**, Selected frame from a fast single-molecule image sequence (left) and corresponding trajectories (right). **c-e,** HMM analysis of diffusive states. Shown is a representative α_{2A}-AR trajectory (**c**), with its displacement (*r*) over time (**d**) and the result of the global HMM analysis (**e**) revealing 4 states (S1-S4, labelled with different colours). **f,** Model and diffusion coefficients (*D;* $\mu m^2\ s^{-1}$) derived from the HMM analysis. Each state is represented by a solid circle; circle area and arrow thickness proportional to occupancy and transition probability, respectively. Differences were statistically significant by two-way ANOVA. *, P<0.05, **, P<0.01, ***, P<0.001, ****, P<0.0001 vs. corresponding state of α_{2A}-AR by Tukey's multiple comparison test. Data are mean±s.d. n=22 (85,475), 13 (47,062) and 28 (110,907) cells (trajectories) for α_{2A}-AR, $G\alpha_i$ and CD86, respectively. Images (**b**, **c**) represent 5 independent experiments.

Figure 2 | Complex diffusion dynamics generates hot spots for receptor:G protein interactions. a, α_{2A}-AR localizations over $G\alpha_i$ potential energy map (left) and quantifications of relative potential energy at the localizations ($V_{L,rel}$; right). **b**, α_{2A}-AR:$G\alpha_i$ interactions over merged α_{2A}-AR and $G\alpha_i$ potential energy (*V*) maps (left) and corresponding quantifications (right).

Arrowheads, localizations concentrated at hot spots. **c-e,** α_{2A}-AR trajectories over images of tubulin (**c**), actin (**d**) or CCPs (**e**) (left) and corresponding colocalization analyses (right). **f**, Trajectories of α_{2A}-ARs (colour-coded according to HMM states) stopping at CCPs (arrowheads; left) and corresponding quantitative analysis (right). **g**, α_{2A}-AR trajectories over actin PALM image (left) and corresponding colocalization analysis (right). Arrowheads, α_{2A}-ARs crossing over actin fibres. **h,** α_{2A}-AR potential energy map over actin PALM image (left) and zoom-in view showing hot spot surrounded by actin fibres (right). α_{2A}-ARs in **g** and **h** were labelled with S647-BG. Results (**a-e**, **g**) were compared to random localizations. See Supplementary Methods for details. Data are mean±s.d. n, number of cells. #, P<0.05, ##, P<0.01, ###, P<0.001, ####, P<0.0001 vs. random localizations by two-sided paired t-test. *, P<0.05, ****, P<0.0001 vs. α_{2A}-AR (basal) by two-sided unpaired t-test. Images (**h**) represent 2 independent experiments.

Figure 3 | Analysis of receptor:G protein interactions. a, Schematic comparison between random colocalizations and true interactions. On average, the observed duration of true interactions (Δt_{obs}) corresponds to their true duration (Δt_{true}) plus that of random colocalizations (Δt_{random}). The distribution of true durations can then be estimated via deconvolution. **b,** Distributions of the estimated durations of α_{2A}-AR:Gα_i interactions under basal and stimulated (NE, 100 μM) conditions, based on deconvolution. CD86 was used as non-interacting control. **c,** Relaxation curves calculated from the data in **b**, showing the dissociation kinetics of α_{2A}-AR:Gα_i complexes (left, linear; right, semilogarithmic plot). **d,** Estimated rate constants of non-productive interactions plus random colocalizations (k_{np+rc}; left), α_{2A}-AR:Gα_i association ($k_{on;}$ middle) and dissociation (k_{off}; mean, 95%CI; right) for the indicated ligands. Differences in k_{on} values are statistically significant by one-way ANOVA. ****, P<0.0001 vs. NE 100 μM by Tukey's multiple comparison test. Differences in k_{off} values vs. NE 100 μM were assessed by two-sided unpaired t-test with Bonferroni correction (****, P<0.0001). **e**, Relaxation curves of α_{2A}-AR:Gα_i interactions obtained with an inverse agonist (yohimbine) or using a PTX-sensitive Gα_i construct. **f**, Relaxation curves of β_2-AR:Gα_s interactions. **g,** Estimated k_{on} and k_{off} (mean, 95%CI) for β_2-AR:Gα_s interactions. ****, P<0.0001 vs. Iso by two-sided unpaired t-test. **h,** Relationship between measured k_{on} and efficacy on α_{2A}-AR activation (mean±s.e.m.). Brackets, affinity values (pK_i). Efficacy and affinity values are from ref. 24. **i,** Apparent interaction between α_{2A}-AR and Gα_i lasting for 1.2 s. After the interaction, the receptor resumes moving, whereas the G protein remains immobile. **j,** α_{2A}-AR and Gα_i trajectories stopping (left) or continuing

moving (right) during apparent interactions. **k,** Distribution of diffusive states (based on HMM analysis) of α_{2A}-AR and $G\alpha_i$ (NE, 100 μM) during apparent interactions (colocalization duration ≥ 1.1 s) compared to time outside interactions. Differences are statistically significant by chi-square test (****, P<0.0001; n=1,265,634 and 527,058 data points for α_{2A}-AR and $G\alpha_i$, respectively). All ligands were used at saturating concentrations, unless otherwise indicated. See Supplementary Methods for details. Data are mean±s.d., unless otherwise indicated. n, number of cells (**d**, **g**). Images (**i, j**) represent 5 independent experiments. N.D., not determinable.

Figure 4 | Hot spots for receptor-G protein signalling. a, Stochastic simulations of receptor:G protein interactions. Left, simulated trajectories. Right, fraction of interacting molecules over time. Compared are results with experimentally measured potential energy (*V*) landscapes vs. simple Brownian motion. **b**, Visualization of local G_s protein activation at the plasma membrane of primary human endothelial cells. Cells were transfected with a fluorescent sensor (Nb37-EYFP) recognizing active, nucleotide-free $G\alpha_s$. Left, β_2-AR localizations over the obtained spatial map of G_s protein activity. Right, quantification. Data are mean±s.d. n, number of cells. ####, P<0.0001 vs. random localizations by two-sided paired t-test.

Methods

Materials

Cell culture reagents, Lipofectamine 2000, Lipofectamine 3000, TetraSpeck fluorescent beads, fluorescein arsenical hairpin binder (FlAsH) and CellMask Green Plasma Membrane Stain were from Thermo Fisher Scientific. The Effectene transfection reagent was from Qiagen. UK-14,304 and clonidine were from Tocris Bioscience. All other GPCR ligands, pertussis toxin (PTX), 1,2-ethanedithiol (EDT) and guanosine 5′-triphosphate (GTP) were from Sigma-Aldrich. [^{35}S]GTPγS was from PerkinElmer. The fluorescent benzyl guanine derivatives SNAP-Surface 549 (S549-BG) and SNAP-Surface Alexa Fluor 647 (S647-BG) were from New England Biolabs. Live-cell fluorogenic probes for actin (SiR-Actin) and tubulin (SiR-Tubulin)[25] were from Spirochrome. The silicon-rhodamine benzyl cytosine derivative (SiR-BC)[26] was kindly provided by Kai Johnsson (Max Planck Institute for Medical Research, Heidelberg, Germany). Ultraclean glass coverslips were obtained as previously described[4].

Molecular biology

A plasmid coding for the N-terminally SNAP-tagged α_{2A}-adrenergic receptor (SNAP-α_{2A}-AR) was generated by inserting the SNAP tag[5] before the coding sequence of the murine α_{2A}-adrenergic receptor. The generation and functional characterization of the N-terminally SNAP-tagged β_2-adrenergic receptor construct (SNAP-β_2-AR) have been described in a previous study[4]. A plasmid (Gα_i-CLIP) coding for the rat Gα_{i1} subunit with the CLIP tag[6] inserted in the αA-αB loop within the α-helical domain (between positions 91 and 92) was generated by replacing YFP with the CLIP tag in a previously described YFP-tagged Gα_{i1} construct[27]. The construct additionally harboured the C351I mutation to render it PTX-insensitive[28]. A plasmid coding for the rat Gα_s subunit with the CLIP tag inserted between positions 72 and 85 (Gα_s-CLIP) was generated by replacing YFP with the CLIP tag in a previously described YFP-tagged Gα_s construct[29]. All tagged receptor and Gα subunit constructs behaved like the corresponding wild type in functional assays (Extended Data Fig. 1a, b). A construct coding for His-tagged Nb37[14] was kindly provided by Jan Steyaert (VIB, Brussels, Belgium). A plasmid coding for the C-terminally EYFP-tagged Nb37 (Nb37-EYFP) was generated by fusing EYFP to the C-terminus of Nb37. Plasmids coding for CD86 with either one or two SNAP tags fused to its N-terminus have been previously described[4]. Plasmids coding for CD86 with either one or two CLIP tags fused to its C-terminus were generated by inserting either one or two copies of the CLIP tag before the stop codon of CD86.

Cell culture and transfection

Chinese hamster ovary K1 (CHO-K1) cells (ATCC) were cultured in phenol red-free Dulbecco's modified Eagle's medium (DMEM)/F-12 supplemented with 5% FCS, 100 U/ml penicillin and 0.1 mg/ml streptomycin at 37 °C, 5% CO_2. For single-molecule experiments, CHO-K1 cells were seeded on ultraclean 24-mm glass coverslips in 6-well culture plates at a density of $3 \cdot 10^5$ cells/well. Cells were treated with 50 ng/ml pertussis toxin (PTX) to inactivate endogenous G$\alpha_{i/o}$ proteins. Transfection was performed 24 h after seeding using Lipofectamine 2000. For each well, 0.8 µg SNAP-α_{2A}-AR or SNAP-β_2-AR, 0.6 µg Gα_i-CLIP or Gα_s-CLIP, 0.4 µg Gβ_1, 0.2 µg Gγ_2, and 6 µL Lipofectamine 2000 were used. Cells were labelled and imaged by single-molecule microscopy 4-6 h after transfection to obtain low physiological expression levels[4]. To label CCPs, cells were transfected 24 h prior to the experiment with GFP-tagged adaptor protein 2 (AP2-GFP), kindly provided by Tom Kirchhausen (Harvard Medical School, USA). Human

embryonic kidney 293 (HEK293) cells (ATCC) were cultured in DMEM supplemented with 5% FCS, 100 U/ml penicillin and 0.1 mg/ml streptomycin at 37 °C, 5% CO_2. HEK293 cells were transfected with Effectene, following the manufacturer's instructions. Cell lines have not been authenticated. Cells were routinely tested for mycoplasma contamination by PCR using specific primers.

For the [^{35}S]GTPγS binding experiments, HEK293 cells were plated in 10-cm culture dishes and transfected with 3.3 μg α_{2A}-AR, 3.3 μg wild-type or CLIP tagged $G\alpha_i$, 2.0 μg $G\beta_1$ and 1.5 μg $G\gamma_2$ plasmids.

For FRET experiments, HEK293 cells were seeded on poly-L-lysine–coated 24-mm coverslips and transfected with the indicated constructs. The α_{2A}-AR-Flash/CFP sensor was used to monitor receptor activation[30]. Co-transfection of α_{2A}-AR-YFP, $G\alpha_i$-CFP, $G\beta_1$ and $G\gamma_2$ was used to monitor G protein recruitment to the receptor[2]. The $G\beta_1$-2A-cpV-$G\gamma_2$-IRES-$G\alpha_{i2}$-mTq2 sensor[31] was used to monitor G_i protein activation.

Human umbilical vein endothelial cells (HUVEC) were purchased from Lonza and cultured in complete EGM-2 BulletKit medium (Lonza). HUVEC were plated on ultraclean 24-mm glass coverslips at a density of $3.5 \cdot 10^5$ cells/well and transfected with Lipofectamine 3000 using the same DNA amounts indicated for CHO cells. HUVEC were cultured for a maximum of 10 passages. To visualize local G_s protein activation at the plasma membrane, HUVEC were transfected 24 h prior to the experiment with the Nb37-EYFP construct.

[^{35}S]GTPγS binding assay

Membrane preparation and [^{35}S]GTPγS binding assay were performed following a previously described protocol[32]. Cells were homogenized in lysis buffer (5 mM Tris, 2 mM EDTA, pH 7.4) and then centrifuged at 1,000xg for 10 min. The supernatant was collected and centrifuged at 50,000xg for 30 min. The remaining pellet was resuspended in binding buffer (100 mM NaCl, 10 mM $MgCl_2$, 20 mM HEPES, pH 7.4). All procedures were performed at 4 °C. Protein concentrations were determined using the Bradford assay. 10 μg membrane proteins were then incubated with the indicated agonist concentrations and 100 pM [^{35}S]GTPγS for 15-300 s. Non-specific binding was evaluated by adding 10 μM GTP. The samples were then passed through glass fibre filters and radioactivity was determined using a liquid scintillation counter (Beckman LS-1801).

Live-cell protein labelling

Cells were labelled with a combination of a cell-impermeable SNAP substrate (S549-BG), to label cell-surface receptors, and a highly cell-permeable CLIP substrate (SiR-BC)[26], to label intracellular G proteins. Cells were incubated with 4 μM S549-BG and 8 μM SiR-BC in complete culture medium for 20 min at 37 °C. Cells were then washed three times using complete culture medium, with 5 min incubation after each wash. This protocol gives labelling efficacy of ~90% and ~80% for extracellular SNAP and intracellular CLIP labelling, respectively (Extended Data Fig. 1c, d).

Actin and tubulin labelling were performed using SiR-actin and SiR-tubulin, respectively, following the manufacturer's protocol. Briefly, cells were labelled with 3 μM SiR-actin or SiR-tubulin in the presence of 10 μM verapamil for 20 min at 37 °C, followed by three washes with complete culture medium.

FlAsH labelling was performed as previously described[30]. Briefly, cells were incubated with 1 μM FlAsH and 12.5 μM EDT in Hank's balanced salt solution (HBSS) for 1 h. The cells were then washed twice with HBSS and incubated with 250 μM EDT in HBSS for 10 min. The cells were washed a third time with HBSS immediately before the FRET measurement.

FRET measurements

Fluorescence resonance energy transfer (FRET) experiments to examine the ensemble kinetics of receptor/G protein signalling in intact cells were done as previously described[2,33,34]. Measurements were performed on an Axiovert 200 inverted microscope (Zeiss) equipped with an oil immersion 100X objective (Plan-Neofluar 100x, N.A. 1.30), a beamsplitter (DCLP505) and a Polychrome IV monochromator and dual-emission photometric system (Till Photonics). Transfected HEK293 cells were placed in a microscopy chamber filled with imaging buffer (137 mM NaCl, 5.4 mM KCl, 2 mM $CaCl_2$, 1 mM $MgCl_2$, 10 mM HEPES, pH 7.3). Agonist stimulation was applied using a pressurized rapid superfusion system (ALA-VM8, ALA Scientific Instruments). FRET was monitored as the ratio between YFP (535±15 nm) and CFP (480±20) emission upon CFP excitation at 436±10 nm. The YFP signal was corrected for direct excitation and bleed-through of CFP emission into the YFP channel as previously described[2].

Single-molecule microscopy and PALM

Single-molecule microscopy experiments were performed using total internal reflection fluorescence (TIRF) illumination on a custom Nikon Eclipse Ti TIRF microscope equipped with 405 nm, 488 nm, 561 nm and 640 nm diode lasers (Coherent), a quadruple band excitation filter, a 100x oil-immersion objective (CFI Apo TIRF 100x, N.A. 1.49), two beam splitters, four separate EMCCD cameras (iXon DU897, Andor), hardware focus stabilization and a temperature control system. Coverslips were mounted in a microscopy chamber filled with imaging buffer. The objective and the sample were maintained at 20 °C by means of a water-cooled inset and objective ring connected to a thermostated water bath. Images in the four channels were acquired simultaneously on the four separate EMCCD cameras. Image sequences (400 frames) were taken in crop and frame-transfer mode, resulting in an acquisition speed of 35 frames/s (i.e. one image every 28 ms).

PALM imaging was performed by TIRF microscopy immediately after the acquisition for single-particle tracking. In this case, cells were additionally transfected 24 h before the experiment with the photoconvertible probe mEOS-LifeAct (a kind gift of Markus Sauer, University of Würzburg, Germany). mEOS was excited at 561 nm, while applying low-intensity 405 nm laser light to induce photoconversion. 10,000 frames were acquired at a speed of 35 frames/s. Superresolved images were then obtained using the rapidSTORM software[35].

Images from different channels were registered against each other using a linear piecewise transformation in *Matlab* based on reference points obtained with multicolour fluorescent beads (TetraSpeck; 100 nm size).

Single particle tracking and subsequent analyses

Single particle detection and tracking were performed using the u-track software[36] in Matlab environment as previously described[4]. The interchannel localization precision after coordinate registration by linear piecewise transformation was ~20 nm. For the analysis of receptor:G protein interactions, a non-related membrane receptor (CD86) with diffusion characteristics comparable to those of the α_{2A}-AR was used as negative control and as reference for random colocalizations[4]. A method based on deconvolution of the observed interaction times with the Lucy-Richardson algorithm[37,38] was then applied to estimate the underlying duration of receptor:G protein interactions (see Supplementary Methods and Extended Data Fig. 7).

To investigate the motion of receptors and G proteins during or immediately before/after an

interaction (Fig. 3i-k and Extended Data Fig. 9c), we considered only apparent interactions with duration ≥ 1.1 s, so that random colocalization represented only a small fraction (approximately 15%), based on a comparison between α_{2A}-AR (NE 100 μM) and CD86 (used as negative control).

Detailed information about the computational analyses can be found in Supplementary Methods.

Hidden Markov model (HMM) analysis

A software based on a variational Bayesian treatment of HMMs (vbSPT)[8] was used to identify discrete diffusive states in the single molecule trajectories and analyse their characteristics. The number of iterations and bootstrapping were set to 25 and 100, respectively. Diffusion coefficients and dwell times derived from the analysis were used to estimate the size of the corresponding nanocompartments on the plasma membrane (see Supplementary Methods).

Spatial mapping of receptor/G protein dynamics

Spatial maps of diffusivity (*D*) and potential energy (*V*) were obtained using the InferenceMAP software[9], based on Bayesian inference, considering a physical model of diffusion in a potential field. Only well-adhering cells with a flat plasma membrane were chosen to avoid artefacts due to uneven distance from the coverslip. The flatness of the plasma membrane was verified by staining with a fluorescent phospholipid (CellMask Green). The analysed areas were partitioned in small regions of variable size by Voronoi tessellation[9]. The number of regions was optimized to avoid areas with low number of localizations. The obtained potential energy maps were subsequently used to perform particle-based stochastic simulations of receptor:G protein interactions (see Supplementary Methods).

Statistics and reproducibility

Statistical analyses were performed using the Prism 6 software (GraphPad Software). Differences between two groups were assessed by two-sided Student´s t-test. Differences among three or more groups were assessed by one-way or two-way analysis of variance (ANOVA), as appropriate, followed by Tukey's multiple comparison test (with the exception of the data in Figure 3d, right, which were compared by two-sided unpaired t-test with Bonferroni

correction). Differences in categorical variables were assessed by chi-square test. Differences were considered significant for P values < 0.05.

Data availability

The data that support the findings of this study are available from the corresponding author upon reasonable request.

Code availability

Matlab scripts are available from the corresponding author upon reasonable request.

25 Lukinavicius, G. *et al.* Fluorogenic probes for live-cell imaging of the cytoskeleton. *Nat. Methods* **11**, 731-733 (2014).

26 Lukinavicius, G. *et al.* A near-infrared fluorophore for live-cell super-resolution microscopy of cellular proteins. *Nat. Chem.* **5**, 132-139 (2013).

27 Frank, M., Thumer, L., Lohse, M. J. & Bunemann, M. G Protein activation without subunit dissociation depends on a $G\alpha_i$-specific region. *J. Biol. Chem.* **280**, 24584-24590 (2005).

28 Bahia, D. S. *et al.* Hydrophobicity of residue 351 of the G protein $G_{i1}\alpha$ determines the extent of activation by the α_{2A}-adrenoceptor. *Biochemistry* **37**, 11555-11562 (1998).

29 Hein, P. *et al.* G_s activation is time-limiting in initiating receptor-mediated signaling. *J. Biol. Chem.* **281**, 33345-33351 (2006).

30 Hoffmann, C. *et al.* A FlAsH-based FRET approach to determine G protein-coupled receptor activation in living cells. *Nat. Methods* **2**, 171-176 (2005).

31 van Unen, J. *et al.* A New Generation of FRET Sensors for Robust Measurement of $G\alpha_{i1}$, $G\alpha_{i2}$ and $G\alpha_{i3}$ Activation Kinetics in Single Cells. *PLoS One* **11**, e0146789 (2016).

32 Traynor, J. R. & Nahorski, S. R. Modulation by μ-opioid agonists of guanosine-5'-O-(3-[35S]thio)triphosphate binding to membranes from human neuroblastoma SH-SY5Y cells. *Mol. Pharmacol.* **47**, 848-854 (1995).

33 Vilardaga, J. P., Bünemann, M., Krasel, C., Castro, M. & Lohse, M. J. Measurement of the millisecond activation switch of G protein-coupled receptors in living cells. *Nat. Biotechnol.*

21, 807-812 (2003).

34 Bünemann, M., Frank, M. & Lohse, M. J. G_i protein activation in intact cells involves subunit rearrangement rather than dissociation. *Proc. Natl. Acad. Sci. U. S. A.* **100**, 16077-16082 (2003).

35 Wolter, S. *et al.* rapidSTORM: accurate, fast open-source software for localization microscopy. *Nat. Methods* **9**, 1040-1041 (2012).

36 Jaqaman, K. *et al.* Robust single-particle tracking in live-cell time-lapse sequences. *Nat. Methods* **5**, 695-702 (2008).

37 Richardson, W. H. Bayesian-Based Iterative Method of Image Restoration. *J. Opt. Soc. Am.* **62**, 55-59 (1972).

38 Lucy, L. B. An iterative technique for the rectification of observed distributions. *Astron. J.* **79**, 745-754 (1974).

Extended Data Figure legends

Extended Data Figure 1 | Control experiments. a-c, Functional characterization of the SNAP/CLIP tagged receptor/G protein constructs. **a**, FRET measurements of G_i protein activation to test the SNAP-tagged α_{2A}-AR construct. HEK-293 cells were co-transfected with a FRET sensor for G_i protein activation ($G\beta_1$-2A-cpV-$G\gamma_2$-IRES-$G\alpha_{i2}$-mTq2) and either wild-type or SNAP-tagged α_{2A}-AR (n=9, 11 cells). Concentration response relationships were obtained from FRET measurements in which the cells were stimulated with increasing concentrations of NE. The SNAP-tagged β_2-AR construct was tested in a previous study[4]. **b**, GTPγS binding assay to test the CLIP-tagged $G\alpha_i$ and $G\alpha_s$ constructs. The corresponding wild-type constructs were used as control. Shown are time courses of GTPγS binding in the presence or absence of agonist (left, clonidine, 10 μM; right, isoproterenol, 10 μM) (n=3 biological replicates per condition). **c**, Efficiency of extracellular labelling with the cell impermeable SNAP substrate S549-BG in cells transfected with CD86 carrying two SNAP tags at its N-terminus (n=28, 13, 17, 14 and 11 cells). **d,** Efficiency of intracellular labelling with the cell permeable CLIP substrate SiR-BC in cells transfected with CD86 carrying two CLIP tags at its C-terminus (n=18, 26, 31, 27 cells). Labelling efficiencies in **c** and **d** were determined by fitting single-particle intensity data with a mixed Gaussian model[4]. The following concentrations were chosen for subsequent experiments: 4 μM S549-BG (labelling efficiency 91.1±2.9%) and 8 μM SiR-BC (labelling

efficiency 82.6±2.1%). **e**, Specificity of labelling. Shown are TIRF images of CHO cells transfected with different combinations of SNAP-α_{2A}-AR and Gα_i-CLIP, followed by labelling with S549-BG or SiR-BC (except for the positive control cotransfected with SNAP-α_{2A}-AR and Gα_i-CLIP, which was labelled with both fluorescent substrates). Unspecific labelling in either mock or cross-transfected cells was responsible for 2-3 spots per cell on average against ~300-400 in the positive controls. This very low number of unspecific immobile localizations (<1%) does not significantly interfere with the analyses of this study. **f,** Representative potential energy (*V*) maps calculated in mock-transfected cells. Shown are results obtained after adding simulated trajectories with Brownian motion to reproduce a condition of diffusing particles over immobile unspecific localizations. The presence of immobile unspecific localizations was not sufficient to generate local low potential energy areas (see **Extended Data Fig. 4b** for comparison). Data are mean±s.e.m. Images (**e, f**) represent 3 independent experiments.

Extended Data Figure 2 | MSD analysis of receptor and G protein trajectories. a, Scatter plot of diffusion coefficient (*D)* and anomalous diffusion exponent (α) values estimated for simulated trajectories with Brownian motion and characteristics similar to those of α_{2A}-ARs. The results were used to set the cut-offs for classifying the trajectories into four groups according to their motion: immobile (D<0.01 $\mu m^2\ s^{-1}$), sub-diffusion (α<0.75), normal diffusion (0.75≤α≤1.25) and super-diffusion (α>1.25). **b,** Scatter plot as in **a** for α_{2A}-AR trajectories. **c,** Representative α_{2A}-AR and Gα_i trajectories classified in the four groups. **d**, Relative frequency distributions of the trajectories in the four groups (left) and corresponding *D* values (right) for receptors and G proteins under basal and stimulated conditions. The control CD86 was expressed together with wild-type α_{2A}-AR and stimulated with NE to verify if the effects observed upon agonist stimulation were specific for Gα_i. Differences in **d** are statistically significant by two-way ANOVA. #, P<0.05, ##, P<0.01 and ####, P<0.0001 vs. the corresponding basal condition and **, P<0.01, ***, P<0.001, ****, P<0.0001, vs. α_{2A}-AR basal (top) or β_2-AR basal (bottom) by Tukey's multiple comparison test. Data are mean±s.e.m. n=30 (9,273), 17 (6,623), 37 (8,309), 30 (4,699), 18 (2,182), 36 (5,240), 28 (11,267), 27 (12,697), 29 (10,760), 47 (16,461), 29 (41,079) and 47 (7,585) cells (trajectories) for α_{2A}-AR basal, α_{2A}-AR NE, α_{2A}-AR UK-14,304, Gα_i basal, Gα_i NE, Gα_i UK-14,304, CD86 basal, CD86 NE, β_2-AR basal, β_2-AR Iso, Gα_s basal, Gα_s Iso, respectively. Images (**c**) represent 5 independent experiments.

Extended Data Figure 3 | Complete results of the hidden Markov model (HMM) analysis. Differences are statistically significant by two-way ANOVA. #, P<0.05, ##, P<0.01, ###, P<0.001 and ####, P<0.0001 vs. the corresponding basal condition, and *, P<0.05, **,P<0.01, ***, P<0.001 and ****: P<0.0001 vs. α_{2A}-AR basal (for Gα_i and CD86) or β_2-AR basal (for Gα_s) by Tukey's multiple comparison test. Data are mean±s.d. n=22 (85,475), 11 (44,797), 31 (153,072), 13 (47,062), 9 (15,161), 30 (88,397), 28 (110,907), 30 (147,222), 27 (142,243), 44 (229,815), 28 (84,668) and 44 (171,623) cells (trajectories) for α_{2A}-AR basal, α_{2A}-AR NE, α_{2A}-AR UK-14,304, Gα_i basal, Gα_i NE, Gα_i UK-14,304, CD86 basal, CD86 NE, β_2-AR basal, β_2-AR Iso, Gα_s basal, Gα_s Iso, respectively. N.D., not determinable.

Extended Data Figure 4 | Complex diffusion dynamics of α_{2A}-AR and Gα_i. a, density maps of α_{2A}-AR and Gα_i localizations (selected trajectories overlaid in different colours; arrowheads, areas of high density). **b**, Potential energy (*V*) maps for α_{2A}-AR and Gα_i, calculated for the same membrane region. **c,** Merge of potential energy maps in **b** (top) and line-profile plot along the dashed line (bottom). Arrowheads, hot spots where *V* is low for both α_{2A}-AR and Gα_i. **d**, Additional examples of α_{2A}-AR potential energy (*V*) maps over actin PALM images and corresponding zoom-in views. Images represent 3 (**a**-**c**) and 2 (**d**) independent experiments.

Extended Data Figure 5 | Complex diffusion dynamics of β_2-AR and Gα_s. a, β_{2A}-AR localizations over Gα_s potential energy (*V*) map and vice versa (top) and quantifications of relative potential energy at the localizations ($V_{L,rel}$; bottom). A negative value indicates relatively lower potential energy at the localizations. **b**, β_2-AR:Gα_s interactions over merged β_2-AR and Gα_s potential energy map (top) and corresponding quantifications (bottom). Arrowheads, localizations concentrated at hot spots. **c-e,** β_2-AR trajectories over images of tubulin (**c**), actin (**d**) or CCPs (**e**) (top) and corresponding colocalization analyses (bottom). Negative colocalization index (*I*) values indicate preferential avoidance of the imaged structures by the receptors. **f,** Trajectory of β_2-AR stopping at CCP (arrowhead; top) and corresponding quantitative analysis (bottom). The trajectory is colour-coded according to the HMM states. Results in **a**-**e** were compared to those obtained with random localizations. See Supplementary Methods for details. Data are mean±s.d. n, number of cells. #, P<0.05, ##, P<0.01, ###, P<0.001, ####, P<0.0001 vs. random localizations by two-sided paired t-test. *, P<0.05, **, P<0.01, ***, P<0.001, ****, P<0.0001 vs. β_2-AR (basal) by two-sided unpaired t-test.

Extended Data Figure 6 | Complex diffusion dynamics of Gα_i. a, Gα_i trajectories over actin PALM image. Arrowheads, Gα_i subunits crossing over actin fibres. **b,** Gα_i trajectories over image of CCPs. **c,** Gα_i potential energy (*V*) map over PALM image of actin fibres (left) and corresponding zoom-in view (right). Images represent 2 (**a**, **c**) and 3 (**b**) independent experiments.

Extended Data Figure 7 | Validation of the analysis of receptor:G protein interactions using simulated data. a-d, Test of the Lucy-Richardson (LR) deconvolution algorithm on data obtained with numerical simulations. A numerical simulation of particles interacting and dissociating following an exponential law (n=20,000 particles; k_{off}=0.7 s^{-1}) was performed. In addition, we considered particles undergoing random colocalizations (also terminating following an exponential law; n=20,000 particles; k=1.75 s^{-1}). **a,** Underlying distribution of the interaction times for the true interactions. **b,** Distribution of the colocalization times for the random colocalizations. **c,** Convolution of the distribution in **a** with that in **b**, corresponding to the observed colocalization times. **d,** Deconvolution of the distribution in **c** with that in **b**. Note that the algorithm was capable of correctly retrieving the distribution of the true interaction times. **e, f,** Simulated two-channel image sequences of particles undergoing transient interactions. A defined fraction of particles in the first channel was simulated to undergo interactions with particles in the second channel. The synthetic image sequences were then analysed using automated particle detection and tracking as for the experimental ones. **e,** Representative frame of a simulated two-colour image sequence. **f,** Trajectories obtained by automated single-particle detection and tracking. **g,** Relaxation curve obtained from simulations of non-interacting particles. **h,** Relaxation curve obtained from simulations of interacting and non-dissociating particles. **i,** Result of the LR deconvolution analysis of the data in **h** with those in **g**. Data were fitted with an exponential decay, used to estimate the rate of premature termination (see Supplementary Methods). **j**, Results of the LR deconvolution analysis on simulated image sequences comparing the input dissociation rate constants (k_{off}) and the ones estimated by the analysis. The results were corrected for premature termination of the interactions as described in Supplementary Methods. All simulations were repeated 3 times with similar results.

Extended Data Figure 8 | Simulations with deterministic model of GPCR signalling. a,

Schematic representation of the model. r, inactive receptor. R, active receptor. L, ligand (agonist). **b,** Model reactions and kinetics parameters used in the simulations. **c, d,** FRET measurements of the ensemble kinetics of α_{2A}-AR activation/deactivation in response to transient agonist stimulation. A sensor consisting in the α_{2A}-AR carrying a FlAsH tag in the third intracellular loop and CFP at the C-terminus was used. Shown are a representative FRET measurement (**c**) and the normalized average of the FRET data (**d**; n=4 cells). **e,** Fitting of model parameters using the measured FRET data for receptor activation/deactivation. **f,** Concentration-response relationships for ligand binding, receptor activation and G protein activation generated with the model. **g, h,** Simulations of GPCR signalling in response to transient agonist stimulation, applying the estimated k_{on} and k_{off} for receptor:G protein interactions to the model. Simulations were performed both considering low (**g**) and high (**h**) receptor/G protein expression levels. **i, j,** FRET measurements of the ensemble kinetics of α_{2A}-AR:Gα_i association/dissociation in response to transient agonist stimulation. A sensor consisting in the α_{2A}-AR carrying YFP at the C-terminus and the Gα_{i1} subunit carrying CFP in the αA-αB loop within the α-helical domain was used. Shown are a representative FRET measurement (**i**) and the normalized average (n=16 cells) of the FRET data (**j**). Association and dissociation time constants (mean, 95%CI) were 44.4 (38.3-52.9) ms and 1.22 (1.16-1.29) s. **k,** Comparison between the FRET data in **j** and the result of simulation with the mathematical model. Data are mean±s.e.m.

Extended Data Figure 9 | Hot spots for receptor:G protein interaction in primary human endothelial cells. a, α_{2A}-AR:Gα_i interactions over merged α_{2A}-AR and Gα_i potential energy (*V*) map (left) and corresponding quantifications (right). Arrowheads, α_{2A}-AR:Gα_i interactions concentrated at hot spots. **b**, Same analysis as in **a** for β_2-AR and Gα_s. ####, P<0.0001 vs. random localizations by two-sided paired t-test. **c**, Distribution of diffusion states (based on HMM analysis) of receptor/G protein trajectories during apparent interactions. Differences are statistically significant by chi-square test (****, P<0.0001; n=2,488,438 and 1,382,193 data points for α_{2A}-AR and Gα_i with NE stimulation; n=1,992,190 and 874,317 data points for α_{2A}-AR and Gα_i with UK-14,304 stimulation; n=5,073,163 and 3,959,938 data points for β_2-AR and Gα_s with Iso stimulation, respectively). Data (**a**, **b**) are mean±s.d. n, number of cells (**a**, **b**).

Extended Data Figure 10 | Schematic summary. a, The complex organization of the plasma

membrane, including barriers provided by actin fibres, microtubules and CCPs, generates hot spots for receptor:G protein interaction and signalling. **b,** Receptors and G proteins undergo random collisions (preferentially within these hot spots), which, via very short-lived encounter complexes, only seldom lead to the formation of productive receptor:G protein (R:G) complexes (low k_{on}). Most of these complexes dissociate with a lifetime of ~1-2 s, while very few are long-lived. Agonists mainly act by increasing the k_{on} for receptor:G protein interactions in a ligand-specific manner. These data suggest that most receptor:G protein complexes are transient and that receptor:G protein interactions are not diffusion limited but rather controlled by the large conformational rearrangements occurring during the formation of productive receptor:G protein complexes. See also Supplementary Discussion.

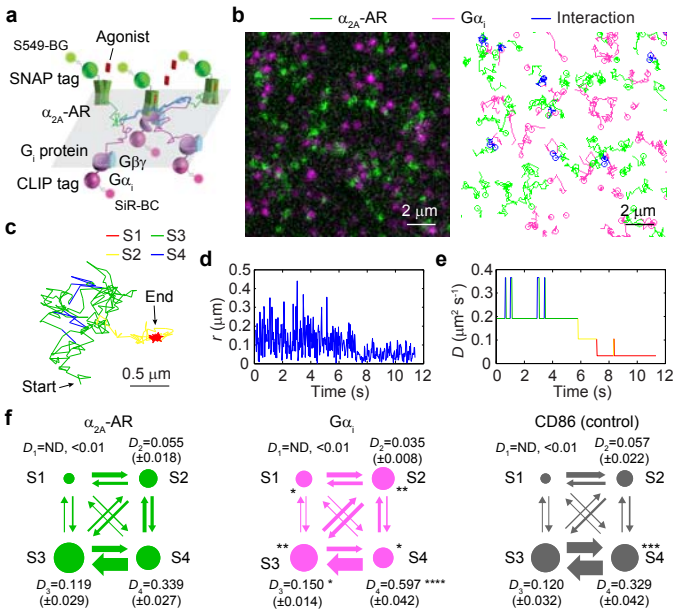
a
S549-BG
Agonist
SNAP tag
α2A-AR
Gi protein
Gβγ
CLIP tag
Gαi
SiR-BC
b
α2A-AR
Gαi
Interaction
2 μm
2 μm
c
S1
S3
S2
S4
End
Start
0.5 μm
d
r (μm)
Time (s)
e
D (μm² s⁻¹)
Time (s)
f
α2A-AR
D1=ND, <0.01
D2=0.055 (±0.018)
D3=0.119 (±0.029)
D4=0.339 (±0.027)
Gαi
D1=ND, <0.01
D2=0.035 (±0.008)
D3=0.150 * (±0.014)
D4=0.597 **** (±0.042)
CD86 (control)
D1=ND, <0.01
D2=0.057 (±0.022)
D3=0.120 (±0.032)
D4=0.329 (±0.042)

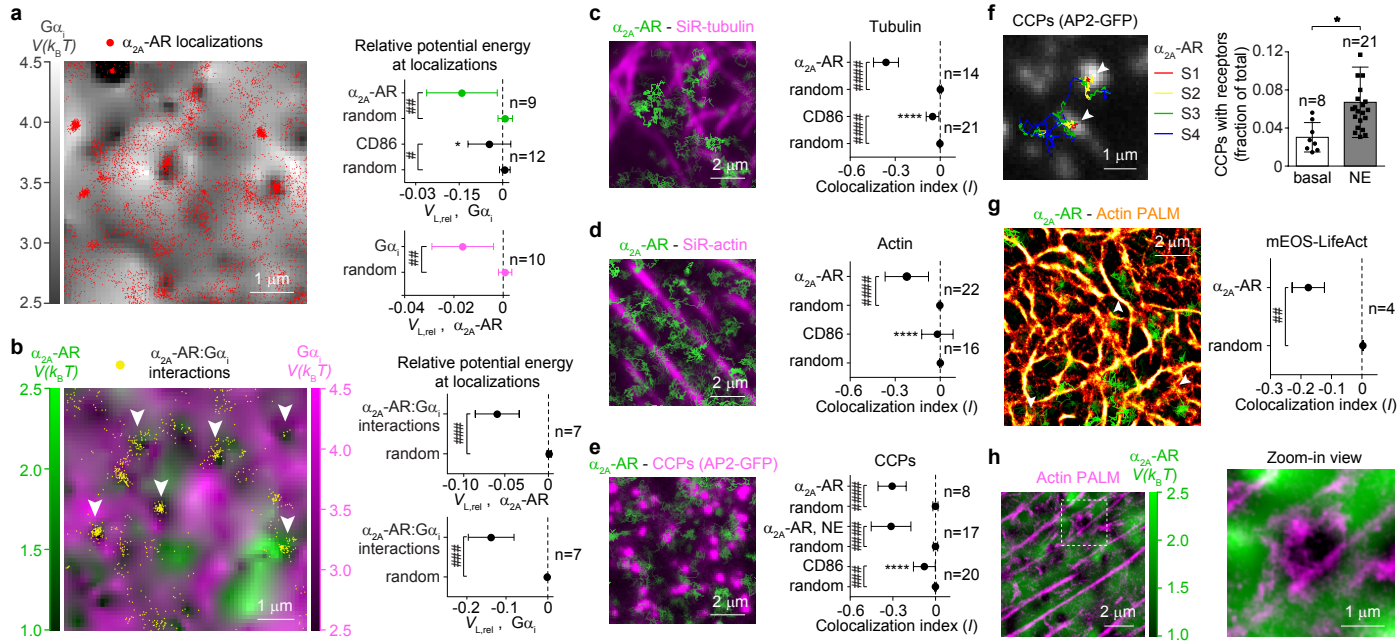
a
Gαi V(kBT)
α2A-AR localizations
1 µm
Relative potential energy at localizations
α2A-AR
random
CD86
random
n=9
n=12
VL,rel , Gαi
Gαi
random
n=10
VL,rel , α2A-AR
b
α2A-AR V(kBT)
α2A-AR:Gαi interactions
Gαi V(kBT)
1 µm
Relative potential energy at localizations
α2A-AR:Gαi interactions
random
n=7
VL,rel , α2A-AR
α2A-AR:Gαi interactions
random
n=7
VL,rel , Gαi
c
α2A-AR - SiR-tubulin
2 µm
Tubulin
α2A-AR
random
CD86
random
n=14
n=21
Colocalization index (I)
d
α2A-AR - SiR-actin
2 µm
Actin
α2A-AR
random
CD86
random
n=22
n=16
Colocalization index (I)
e
α2A-AR - CCPs (AP2-GFP)
2 µm
CCPs
α2A-AR
random
α2A-AR, NE
random
CD86
random
n=8
n=17
n=20
Colocalization index (I)
f
CCPs (AP2-GFP)
1 µm
α2A-AR
S1
S2
S3
S4
CCPs with receptors (fraction of total)
n=8
n=21
basal
NE
g
α2A-AR - Actin PALM
2 µm
mEOS-LifeAct
α2A-AR
random
n=4
Colocalization index (I)
h
Actin PALM
α2A-AR V(kBT)
2 µm
Zoom-in view
1 µm

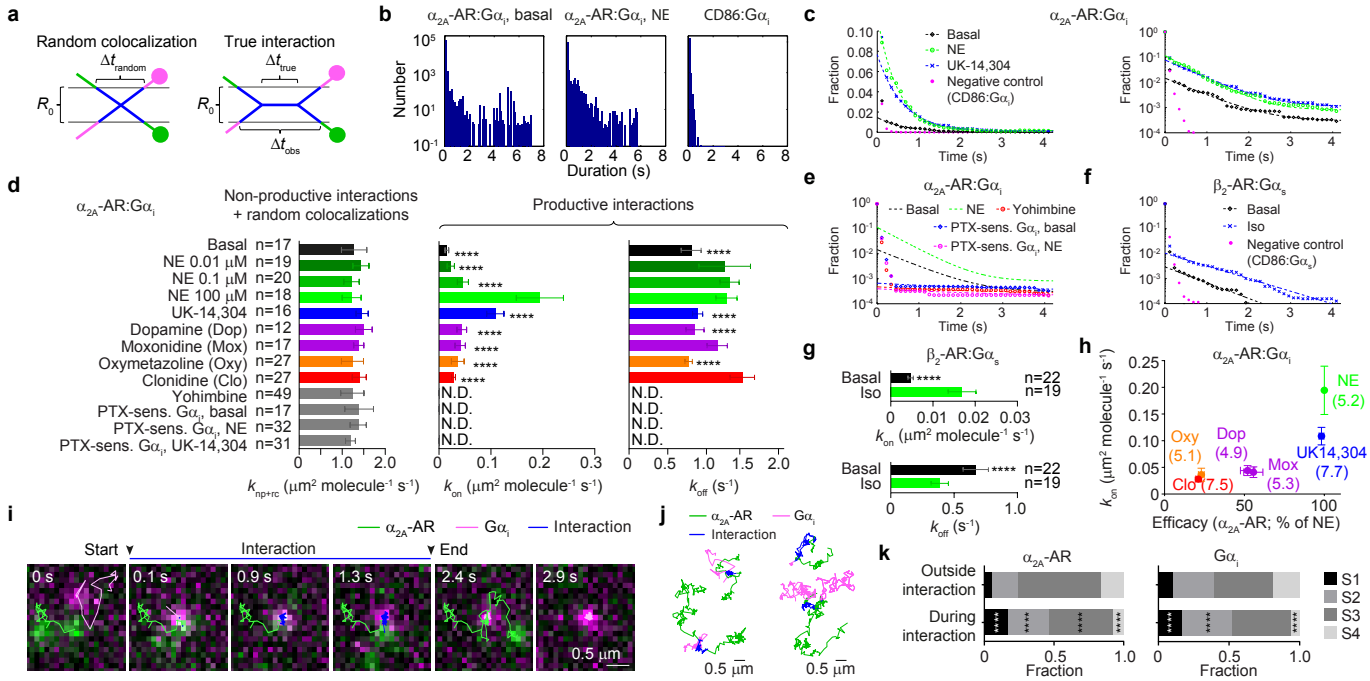
a
Random colocalization
True interaction
b
c
d
Non-productive interactions + random colocalizations
Productive interactions
Basal n=17
NE 0.01 µM n=19
NE 0.1 µM n=20
NE 100 µM n=18
UK-14,304 n=16
Dopamine (Dop) n=12
Moxonidine (Mox) n=17
Oxymetazoline (Oxy) n=27
Clonidine (Clo) n=27
Yohimbine n=49
PTX-sens. Gαi, basal n=17
PTX-sens. Gαi, NE n=32
PTX-sens. Gαi, UK-14,304 n=31
N.D.
Duration (s)
Time (s)
Fraction
Number
e
f
g
h
Basal
Iso
NE (5.2)
Oxy (5.1)
Dop (4.9)
Mox (5.3)
UK14,304 (7.7)
Clo (7.5)
Efficacy (α2A-AR; % of NE)
i
Start
Interaction
End
0 s
0.1 s
0.9 s
1.3 s
2.4 s
2.9 s
0.5 µm
j
k
Outside interaction
During interaction
S1
S2
S3
S4
Fraction

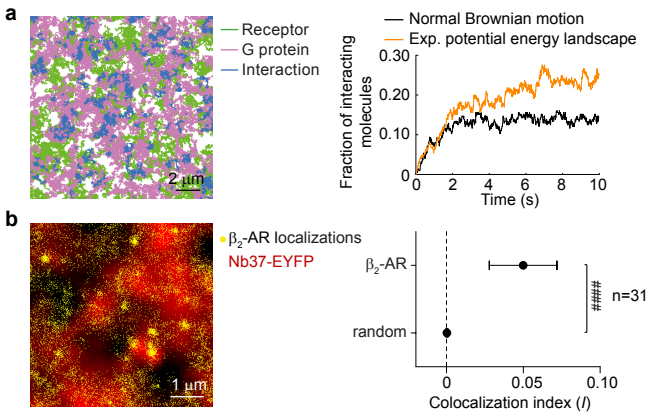
a
Receptor
G protein
Interaction
2 µm
Normal Brownian motion
Exp. potential energy landscape
Fraction of interacting molecules
0.30
0.20
0.10
0
0
2
4
6
8
10
Time (s)
b
β2-AR localizations
Nb37-EYFP
1 µm
β2-AR
random
n=31
0
0.05
0.10
Colocalization index (I)